Published in final edited form as:
DNA Repair (Amst). 2013 December ; 12(12): . doi:10.1016/j.dnarep.2013.09.007.

Coordination of MYH DNA glycosylase and APE1 endonuclease activities via physical interactions

Paz J. Luncsford[‡], **Brittney A. Manvilla**[‡], **Dimeka N. Patterson**[‡], **Shuja S. Malik**[‡], **Jin Jin**[‡], **Bor-Jang Hwang**[‡], **Randall Gunther**[‡], **Snigdha Kalvakolanu**[‡], **Leonora J. Lipinski**[‡], **Weirong Yuan**[£], **Wuyuan Lu**[‡,£], **Alexander C. Drohat**[‡,§], **A-Lien Lu-Chang**[‡,§], and **Eric A. Toth**[‡,§,¥,*]

[‡]Department of Biochemistry and Molecular Biology, University of Maryland School of Medicine, Baltimore, Maryland 21201

[£]Institute of Human Virology, University of Maryland School of Medicine, Baltimore, Maryland 21201

[§]Marlene and Stewart Greenebaum Cancer Center, University of Maryland School of Medicine, Baltimore, Maryland 21201

[¥]Center for Biomolecular Therapeutics, University of Maryland School of Medicine, Baltimore, Maryland 21201

Abstract

MutY homologue (MYH) is a DNA glycosylase which excises adenine paired with the oxidative lesion 7,8-dihydro-8-oxoguanine (8-oxoG, or G°) during base excision repair (BER). Base excision by MYH results in an apurinic/apyrimidinic (AP) site in the DNA where the DNA sugar-phosphate backbone remains intact. A key feature of MYH activity is its physical interaction and coordination with AP endonuclease I (APE1), which subsequently nicks DNA 5' to the AP site. Because AP sites are mutagenic and cytotoxic, they must be processed by APE1 immediately after the action of MYH glycosylase. Our recent reports show that the interdomain connector (IDC) of human MYH (hMYH) maintains interactions with hAPE1 and the human checkpoint clamp Rad9-Rad1-Hus1 (9-1-1) complex. In this study, we used NMR chemical shift perturbation experiments to determine hMYH-binding site on hAPE1. Chemical shift perturbations indicate that the hMYH IDC peptide binds to the DNA-binding site of hAPE1 and an additional site which is distal to the APE1 DNA-binding interface. In these two binding sites, N212 and Q137 of hAPE1 are key mediators of the MYH/APE1 interaction. Intriguingly, despite the fact that hHus1 and hAPE1 both interact with the MYH IDC, hHus1 does not compete with hAPE1 for binding to hMYH. Rather, hHus1 stabilizes the hMYH/hAPE1 complex both *in vitro* and in cells. This is consistent with a common theme in BER, namely that the assembly of protein-DNA complexes enhances repair by efficiently coordinating multiple enzymatic steps while simultaneously minimizing the release of harmful repair intermediates.

[*]Address correspondence to: Eric A. Toth, Department of Biochemistry and Molecular Biology, University of Maryland School of Medicine, 108 N. Greene St., Baltimore, MD 21201, Tel: (410)706-5345, Fax: (410)706-8297, etoth@som.umaryland.edu.

Conflict of interest statement
The authors declare that there are no conflicts of interest.

Keywords

Base excision repair; regulatory protein interactions; DNA glycosylase; AP endonuclease; checkpoint clamp

1. Introduction

Reactive oxygen species of endogenous and environmental origin continuously cause single-base modifications in genomic DNA [1]. Base excision repair (BER) is the major pathway that protects the genome from the mutagenic and cytotoxic effects of such nucleobase damage [2]. Damage-specific DNA glycosylases initiate BER by cleaving the *N*-glycosidic bond between the damaged base and the sugar-phosphate backbone, creating an apurinic/apyrimidinic (AP) site in the DNA [3]. Universal repair enzymes take over to complete repair with synthesis of either a single-nucleotide (SN) patch [4] or a long-patch (LP), consisting of 2–13 nucleotides [5]. AP endonuclease 1 (APE1) is an essential multifunctional enzyme that cleaves the phosphodiester bond 5′ to an AP site generated by DNA glycosylases in both the SN- and LP-BER subpathways [3].

7,8-dihydro-8-oxoguanine (8-oxoG, or G°), generated by the oxidation of guanine, is one of the most prevalent oxidative lesions and is repaired by BER [6]. If DNA replication occurs prior to the repair of the G° lesion, replicative DNA polymerases frequently misincorporate adenine opposite G°. Human MutY homologue (hMYH) is the DNA glycosylase responsible for excising misincorporated adenines to initiate repair of A/G° lesions. Notably, germline mutations of *hMYH* cause the colorectal cancer predisposition syndrome, MYH-associated polyposis (MAP) [7] and the identification of MAP established the first connection between inherited BER defects and cancer [8].

Because AP sites are mutagenic and cytotoxic [8], they must be recognized and processed by APE1 immediately after the action of a DNA glycosylase. A “passing-the-baton” model has been proposed for BER [9], consistent with findings that APE1 interacts with many DNA glycosylases [10–13]. So far, only hMYH has been demonstrated to form a stable complex with APE1 [14], and thus provides an excellent system to study their interaction. A key unanswered question in BER is how the pathway as a whole can be coordinated. Thus far, several candidates have emerged as potential “central coordinators” of BER. In particular, the LP-BER enzymes proliferating cell nuclear antigen (PCNA) and flap endonuclease 1 (FEN1) also physically associate with hAPE1 [15], suggesting that APE1 might be a central coordinator of BER. However, PCNA also interacts with a multitude of enzymes including LP-BER enzymes hMYH [14], DNA polymerases β [16], δ, and ε, replication factor C, FEN1, and DNA ligase I [17, 18], implicating it as another potential coordinator and regulator of LP-BER. The heterotrimeric Rad9-Rad1-Hus1 (9-1-1) complex is a DNA clamp that shows striking structural similarity to PCNA [19–21]. 9-1-1 also physically interacts with many LP-BER enzymes including hMYH [22], hTDG [23], hNEIL1 [24], OGG1 [25], hAPE1 [26], polymerase β [27], FEN1 [28, 29], and Lig1 [30, 31] and therefore is also poised as a likely candidate to coordinate the enzymatic steps of BER.

The physical interaction between MYH and APE1 has been demonstrated by co-immunoprecipitation and GST-pulldown assays [14]. The binding site of APE1 on hMYH has been mapped to residues 295 – 318 of the flexible interdomain connector (IDC) of hMYH [14, 32]. Two groups [13, 33] have shown that a large excess of hAPE1 stimulates the glycosylase activity of MYH. However, the origins of this effect remain unclear. In particular, the binding surface(s) used by APE1 to interact with MYH remains to be identified. To address this issue, we used NMR chemical shift perturbation experiments and

a synthetic IDC peptide (IDC_{pep}) to identify APE1 residues that contact the IDC region of hMYH. Here, we report that hMYH physically interacts with hAPE1 at the APE1 DNA-binding site and another site distal to the APE1 DNA-binding interface. We hypothesize that the physical interaction between hMYH and hAPE1 is one of several regulatory mechanisms that ensures the BER pathway proceeds to completion to avoid the release of toxic intermediates. We validated these findings by demonstrating that alanine mutants of N212 and Q137, two APE1 residues that exhibit significant IDC_{pep}–induced chemical shift perturbations significantly impair the binding of APE1 to MYH. Moreover, addition of either the IDC peptide or hMYH(65–350) to an APE1 endonuclease reaction generates a modest but reproducible enhancement of APE1 activity. Because APE1 and the Rad9-Rad1-Hus1 (9-1-1) complex both interact with the IDC of MYH [14, 22, 32], we sought to determine whether these interactions are mutually exclusive. Toward that end, we examined the effects of the hHus1 subunit of the 9-1-1 complex on MYH/APE1 interactions. Surprisingly, hHus1 enhances binding between hMYH and hAPE1. Thus, we propose that 9-1-1 might coordinate safe and efficient BER by assembling hMYH, hAPE1, and other enzymes as a multiprotein complex on damaged DNA.

2. Materials and Methods

2.1. DNA Purification

The oligodeoxynucleotides (ODN) used to make a DNA duplex containing a guanine opposite an abasic site analog (F/G) for the APE1 repair assay were synthesized (trityl-on) at the Keck Foundation Biotechnology Resource Laboratory, Yale University. The ODNs were purified with Glen-Pak cartridges (Glen Research) and their concentration was determined by absorbance. Duplex DNA was hybridized by heating to 80 °C followed by slow cooling to room temperature.

The duplex DNA is composed of 5'-AGTGCGTCC*F*CGACGAC, where *F* is a tetrahydrofuran abasic site analog, and its complement, 5'-GTCGTCGGGGACGCACT. Oligonucleotides from Integrated DNA Technologies were also used to create a DNA duplex with a thymine base opposite a tetrahydrofuran abasic site analog (F/T). The duplex DNA is composed of 5'-GCTCA*F*GTACAGAGCTGC and its complement, 5'-GCAGCTCTGTACTTGAGC. The DNA strands were annealed as described [34].

2.2. Creation of expression constructs

The sequences of all constructs were verified before undertaking subsequent experiments.

$hAPE1^{\Delta N38}$—The $APE1^{\Delta N38}$ expression plasmid encodes for truncated human APE1, lacking the first 38 residues of the intact protein. The plasmid was constructed as described [35]. In summary, PCR was used to amplify the gene sequence corresponding to residues 39–318 of human APE1 from an expression plasmid harboring the intact gene. The PCR product was then subcloned into the *NheI* and *BamH*I sites of a pET-28 plasmid (Novagen).

hMYH(65–350)—The hMYH(65–350)-pET19b-pps expression construct has been described [32].

hAPE1, hAPE1-N212A, hAPE1-Q137A—hAPE1 in the pET-28 expression plasmid was a kind gift to the laboratory of Dr. Alex Drohat from Professor Ian Hickson of the University of Oxford. The N212A and Q137A mutants were constructed and their sequences confirmed by Genscript (Piscataway, NJ).

GST-hMYH(1–350)—The cDNA fragments containing residues 1–350 of hMYH fused to the GST gene were obtained by PCR and ligated into the pGEX-4T-2 vector (GE Healthcare) as described [22].

GST-hMYH(1–350)-V315A—The V315A mutant of hMYH(1–350) was constructed by the PCR splicing overlap extension method as described [22, 36].

hHus1—The hHus1-pET-21a expression plasmid was constructed as described [22]. The hHus1 gene is fused with a gene sequence that encodes for a C-terminal hexahistidine tag.

hHus1-N1—The hHus1 deletion construct containing residues 1–146 was obtained by PCR using pET-21-hHus1 plasmid [22] as template and the primers Chang390 (5'-GGTCGCGGATCCATGAAGTTTCGGGCCAAGATC-3') and Chang576 (5'-CGCTCTCGAGTAAGTCCTTCCACAATTTCCTTGG-3'). The PCR product was cleaved by BamHI and XhoI into two fragments due to the internal XhoI site at the hHus1 gene. The larger fragment containing residues 1–90 was ligated into pET-21a (EMD Biosciences) to obtain the clone pET21a-hHus1-N1. The hHus1-N1 protein was tagged with His at its C-terminus.

2.3. Protein expression and purification

^{15}N-labeled APE1$^{\Delta N38}$, and unlabeled APE1, APE1-N212A, and APE1-Q137A—To produce uniformly ^{15}N-labeled protein, APE1$^{\Delta N38}$ was expressed as previously described [35]. Briefly, BL21(DE3) cells (Novagen) were transformed with the pET-28 expression plasmid harboring APE1$^{\Delta N38}$, plated, and incubated overnight at 37 °C. A 50-mL starter culture with Luria Broth (LB) medium was grown at 37 °C to an $A_{600} \approx 0.6–0.8$ before transferring cells to 2 L of 3-(N-morpholino)propanesulfonic acid (MOPS) minimal media supplemented with Uniform-[^{15}N]-NH_4CL (1 g/L). The cells were grown at 37 °C until the optical density reached an $A_{600} \approx 0.6$. Protein expression was induced with 0.4 mM isopropyl-1-thio-β-D-galactopyranoside (IPTG) at 16 °C for 12–14 hours. Unlabeled wild-type APE1, APE1-N212A, and APE1-Q137A were produced using the same protocol, with the exception that the bacteria harboring plasmids for these proteins were grown in LB media.

Protein purification was performed at 4 °C as described [35, 37]. Nickel-sepharose affinity chromatography (GE Healthcare) was followed by overnight thrombin cleavage of the N-terminal hexahistidine tag. Ion exchange chromatography using a 5-ml HiTrap SP HP column (GE Healthcare) was the final purification step. The protein was dialyzed into 2 L of NMR buffer consisting of 20 mM sodium phosphate (pH 6.5), 100 mM NaCl, 0.5 mM DTT, and 0.2 mM EDTA. The first dialysis step was performed at room temperature for 4 hours before transferring the protein to 2 L of fresh NMR buffer for further dialysis overnight at 4 °C. APE1$^{\Delta N38}$ was concentrated using centrifugal devices (Sartorius Stedim), and the final protein concentration was determined by absorbance ($\varepsilon^{280} = 56.4\ mM^{-1}cm^{-1}$). The protein was generally used immediately for NMR experiments but was occasionally stored at −80 °C for later use.

His-APE1—BL21(DE3) cells (Novagen) were transformed with hAPE1-pET28. Cells were grown at 37 °C to an $A_{600} \approx 0.6–0.8$ and protein expression was induced with 0.4 mM IPTG at 16 °C overnight. Protein purification was performed at 4 °C. Nickel-sepharose affinity chromatography (GE Healthcare) was followed by anion exchange chromatography using a 12-ml Uno-S column (Bio-Rad). The protein was concentrated using centrifugal devices (Sartorius Stedim) and quantified by a Bradford (Bio-Rad) assay [38]. The protein was either used immediately for experiments or flash-frozen and stored at −80 °C.

hMYH(65–350)—The protein was expressed and purified as described in [32].

hHus1—*E. coli* Rosetta™ 2(DE3) cells (Novagen) were transformed with hHus1-pET-21a [22]. Cells were grown at 37 °C to an $A_{600} \approx 0.6–0.8$ and protein expression was induced with 0.4 mM IPTG at 25 °C overnight. Protein purification was performed at 4 °C as described [22]. In summary, nickel-sepharose affinity chromatography (GE Healthcare) was followed by heparin affinity chromatography (GE Healthcare). The protein was concentrated using centrifugal devices (Sartorius Stedim) and quantified by a Bradford (Bio-Rad) assay [38]. The protein was flash-frozen and stored at −80 °C.

hHus1-N1—The *E. coli* Rosetta cells (Novagen) that harbor the expression plasmid of hHus1-N1 protein were grown and induced as described for GST-hMYH [22]. The hHus1-N1 protein was purified by Ni-NTA resin (QIAGEN) under native conditions according to the manufacturer's protocol. The hHus1-N1 protein eluted from the Ni column was diluted with buffer A (20 mM potassium phosphate (pH 7.4), 0.1 mM EDTA, 10% glycerol, 0.5 mM dithiothreitol and 0.1 mM phenylmethulsulfonyl fluoride) containing 50 mM KCl and further purified by a 1 ml Heparin column (GE Healthcare) equilibrated with buffer A. Upon washing with 5 ml of equilibration buffer, the column was eluted with a 30-ml linear gradient of KCl (0.05–0.8 M) in buffer A. The fractions that contain the hHus1-N1 protein eluted at 0.4 M KCl. This was confirmed by SDS-PAGE. The fractions were then divided into small aliquots and stored at −80°C. The protein concentration was determined by the Bradford method [38].

hMYH IDC peptide (the interdomain connector, residues 293–351 of hMYH)—Residues 293–351 of hMYH correspond to the interdomain connector (IDC). This peptide was synthesized by solid phase chemical synthesis, as described [39], at the Institute of Human Virology at the University of Maryland, Baltimore. The purity of the peptide was verified by HPLC analysis and lyophilized to a powder. The peptide was resuspended in NMR buffer (20 mM sodium phosphate pH 6.5, 100 mM NaCl, 0.5 mM DTT, and 0.2 mM EDTA). PD MiniTrap G-10 columns (GE Healthcare) were used as recommended by the manufacturer for complete exchange into NMR buffer. A sample of our peptide was sent to BioSynthesis for quantitative amino acid analysis and determination of its extinction coefficient at 280 nM ($\varepsilon^{280} = 4819\ M^{-1}cm^{-1}$).

2.4. Nuclear magnetic resonance spectroscopy

NMR spectra were collected at 25 °C on a Bruker AVANCE 800 NMR spectrometer (800.27 MHz for protons) equipped with a 5 mm triple-resonance cryogenic probe with z-axis pulse field gradients. Uniformly ^{15}N-labeled APE1$^{\Delta N38}$ was used to collect two-dimensional heteronuclear single quantum coherence (HSQC) spectra of APE1$^{\Delta N38}$, alone and with the hMYH IDC peptide. The NMR samples contained 0.2 mM APE1$^{\Delta N38}$ in NMR buffer with 7 – 10% D_2O. The hMYH IDC peptide was incrementally added to complete the NMR titration experiment. NMR data were collected for 0.2 mM APE1$^{\Delta N38}$ alone and with the following molar ratios with the IDC peptide: 1:1, 1:2, 1:4, and 1:8. The ^{1}H chemical shifts were referenced to external DSS, and the ^{15}N-shifts were referenced indirectly to liquid ammonia using $^{15}N/^1H = 0.101329118$. NMR data were processed with NMRPipe [40] and analyzed with Sparky [41]. Chemical shift perturbations were tabulated for each APE1$^{\Delta N38}$ residue using equation 1:

$$\Delta = \sqrt{\Delta\delta_{H-N}^2 + (0.1\Delta\delta_N)^2} \quad \text{Eq.1}$$

where Δ is the weighted chemical shift perturbation which utilizes a scaling factor of 0.1 to empirically scale the ^{15}N chemical shift changes to be more equivalent to the ^{1}H chemical

shift changes. The scaling factor is the ratio of the magnetogyric ratios (denoted by the symbol, γ) of the ^{15}N and ^{1}H nuclei ($^{15}N\ \gamma/^{1}H\ \gamma \approx 0.1$). $\Delta\delta_{H\text{-}N}$ refers to the amide proton (^{1}H) chemical shift and $\Delta\delta_{N}$ refers to the ^{15}N chemical shift [42].

2.5. GST-pulldown assays

The GST-pulldown assay was similar to the experiments previously described [14]. Briefly, the GST-tagged hMYH constructs [hMYH(1–350) and hMYH(1–350)-V315A] were grown at 25 °C in *E. coli* Rosetta™ 2(DE3) cells (Novagen) to an $A_{600} \approx 0.6$. Protein expression was induced with 0.4 mM IPTG at 20°C for about 16 hours. The GST-tagged hMYH proteins from the cell lysate were immobilized on Glutathione Sepharose 4 Fast Flow (GE Healthcare) in Buffer G (50 mM Tris-HCl, pH 7.4, 2 mM EDTA) supplemented with 0.15 M NaCl and 0.1 % NP-40. The beads, containing approximately 200 ng of hMYH protein, were incubated with 100 ng of His-tagged APE1 for 16 hours at 4 °C. A control was performed concurrently with immobilized GST alone. To eliminate the effect of nucleic acid on protein-protein interactions, 50 μg/ml of ethidium bromide was added to the immobilized hMYH at 4°C for 30 min prior adding APE1 or Hus1. To test the effect of Hus1 on the MYH-APE1 interaction, purified hHus1 was incubated with the GST-hMYH beads and hAPE1. In separate samples, hHus1 was added in a 1:1 and 1:10 (hAPE1:hHus1) molar ratio with hAPE1. A control pull-down reaction was performed without hHus1. After centrifugation at 3,500 rpm for 2 minutes, the pellets were washed four times with buffer G containing 0.1% NP-40 and 0.15 M NaCl. For pulling down the untagged wild-type, N212A, and Q137A APE1 mutants, we employed the same protocol as above with the exception that the binding buffer contained 0.2 % NP-40 and 0.15 M NaCl and the wash buffer contained 0.2 % NP-40 and 0.3 M NaCl. The supernatants and pellets were fractionated on a 12% SDS-PAGE gel and transferred to a nitrocellulose membrane. Western blot analysis was performed using a monoclonal antibody against hAPE1 (Abcam) and ECL® (enhanced chemiluminescence) detection (GE Healthcare) according to the manufacturer's protocol.

2.6. AP endonuclease assay for APE1

The AP endonuclease activity of APE1 (1 nM) was determined under steady-state conditions with abasic DNA substrate (1 μM) in the presence or absence of the MYH IDC (100 μM), truncated hMYH(65–350) (10 μM), or BSA (1–100 μM). Reactions were performed at 37 °C in HEMN.1 buffer (0.02 M HEPES pH 7.5, 0.2 mM EDTA, 2.5 mM $MgCl_2$, 0.1 M NaCl). For the MYH IDC stored in NMR buffer (20 mM sodium phosphate pH 6.5, 100 mM NaCl, 0.5 mM DTT, 0.2 mM EDTA), and hMYH(65–350) in storage buffer (50 mM Tris pH 7.5, 150 mM NaCl, 1 mM DTT, 1 mM EDTA), equivalent volumes of each buffer were added to control reactions. Reactions were initiated by adding substrate [duplex F/G for peptide; duplex F/G and F/T for hMYH(65–350)] to an equilibrated buffer (5 min, 37 °C) containing APE1, with or without the MYH IDC/ hMYH(65–350). Samples were removed at varying time-points and quenched with 0.1 M NaOH, 0.01 M EDTA (final concentration). The reaction progress (product concentration) for each sample was determined by analytical HPLC, as described previously [34]. Initial velocities (v_0) were determined by fitting the data (product concentration versus time) using linear regression, and were converted to k_{obs} (= v_0/[enzyme]).

2.7. Determination of protein stability by chemical denaturation

The thermodynamic stability of folding was determined by equilibrium denaturation in the presence of varying concentrations of guanidinium HCl (GuHCl). Wild-type APE1, APE1-N212A, and APE1-Q137A proteins were incubated for 20 minutes at 25 °C at a final concentration of 0.4 μM in buffer D (0.02 M HEPES, pH 7.5, 0.1 M NaCl, 0.2 mM EDTA,

2.5 mM $MgCl_2$, 0 to 6 M GuHCl). The extent of unfolding at each GuHCl concentration was determined by measuring the wavelength at which maximal fluorescence emission (λ_{max}) is observed following excitation of tryptophan residues (λ_{ex} = 295 nm). These data were acquired using a Cary Eclipse spectrofluorometer and each experiment was performed in triplicate. GuHCl-induced denaturation was modeled as a two-state transition between native (N) and unfolded (U) states, which exhibit unique maximal emission wavelengths λ_{max}^{N} and λ_{max}^{U} The thermodynamics of GuHCl-induced unfolding were determined by fitting the dependence of λ_{max} on [GuHCl] to equation 2 [43, 44] using non-linear regression and the program Grafit5 [45]:

$$\lambda_{max}=\lambda_{max}^{N}-((\lambda_{max}^{N}-\lambda_{max}^{U})e^{-\Delta G_u/RT})/(1+e^{-\Delta G_u/RT}) \quad \text{Eq. 2}$$

Where $\Delta G_u = \Delta G_{uw} - m_{eq}[GuHCl]$. ΔG_u represents the free energy of protein denaturation at each concentration of GuHCl. ΔGuw is the extrapolated free energy of unfolding in the absence of denaturant, and m_{eq} relates to the sensitivity of ΔG_u to the GuHCl concentration.

2.8. Cell culture, cell extracts, and co-immunoprecipitation

Hus1$^{-/-}$*p21*$^{-/-}$+GFP, and *Hus1*$^{-/-}$*p21*$^{-/-}$+Hus1 mouse embryonic fibroblast (MEF) cells [46] (obtained from Dr. Robert S. Weiss at Connell University) were maintained in Dulbecco's modified Eagle's medium supplemented with 10% fetal bovine serum, 1.0 mM L-glutamine, 0.1 mM MEM non-essential amino acids, 100 μg/ml streptomycin and 100 U/ml penicillin. Cells (10^6–10^7) from 10 cm dishes were harvested, washed with phosphate-buffered saline (PBS), and lysed by using 1 ml of lysis buffer [50 mM Tris HCl, pH 7.4, 120 mM NaCl, 1 mM EDTA, 0.1 % NP-40, and 10 μl protease inhibitor cocktail (P8340, Sigma-Aldrich)]. The whole cell extracts were quickly frozen using liquid nitrogen and stored at −80°C. The protein concentration was determined by Bradford method (Bio-Rad) [38].

Cell extracts (2 mg) were precleared by adding 30 μl protein G plus protein A agarose (Calbiochem IP05) for 2 hours at 4°C. After centrifugation at 1000 x g, the supernatant was incubated with 4 μg of APE1 antibody overnight at 4°C. Protein G plus protein A agarose (30 μl) was added and incubated for 4 hours at 4°C. After centrifugation at 1000 x g, the supernatant was saved and the pellet was washed. The pellet fractions were resolved on a 10% SDS-PAGE. Western blot analysis was performed with hMYH antibody (α344) [47], probed with anti-rabbit HRP- conjugated secondary antibody, and detected by the Enhanced Chemiluminescence (ECL) analysis system (USB Corporation) according to the manufacturer's protocol.

3. Results

3.1. The hMYH interdomain connector (IDC) physically interacts with two binding sites on APE1, one of which overlaps the DNA-binding site

APE1 associates with a number of BER proteins via both physical and non-physical interactions [reviewed by Fan and Wilson [2]]. However, the protein-binding sites on APE1 have not been determined. Manvilla *et al*. [35] recently published the backbone chemical shift assignments for residues 39–318 of hAPE1 (hAPE1$^{\Delta N38}$). The 38 N-terminal residues of hAPE1 are disordered and are not required for its AP endonucleolytic activity [48–50]. The APE1-binding site of hMYH has been determined to include residues 295–318 of hMYH [14]. Residues 295–318 are at the N-terminus of the hMYH IDC domain, and our recent crystal structure of hMYH(65–350) shows that the IDC provides a readily accessible scaffold for proteins to interact with hMYH [32]. To map the hMYH-binding site on APE1, we used NMR to monitor chemical shift perturbations of $^{15-}$N-labeled hAPE1$^{\Delta N38}$ induced by a peptide corresponding to the IDC (residues 293–351) of hMYH. To eliminate chemical

shift perturbations due to changes in pH or ionic strength, hAPE1$^{\Delta N38}$ and the IDC peptide were thoroughly equilibrated in the same preparation of NMR buffer. We collected heteronuclear spin quantum coherence (^{15}N-HSQC) spectra (25 °C) for samples containing hAPE1$^{\Delta N38}$ alone (0.2 mM) and with the IDC peptide in molar ratios of, 1:1, 1:2, 1:4, and 1:8 (APE1:IDC$_{pep}$). The data show that the IDC peptide produces significant chemical shift perturbations in hAPE1$^{\Delta N38}$. Figures 1 and 2 show spectra from the four titrations, and highlight the chemical shift perturbations for hAPE1$^{\Delta N38}$ residue N212 and Q137, respectively. The NMR spectra of hAPE1 $^{\Delta N38}$ alone are shown in red and the increasing IDC titrations are indicated in orange, green, blue, and purple. The combined ^{1}H-^{15}N chemical shift perturbations for nine APE1 residues are given in Table 1. These residues are those most perturbed by the IDC peptide, and exhibit significant shift perturbations at a 2:1 molar ratio (IDC$_{pep}$:hAPE1$^{\Delta N38}$). Residues N212 and G231 also show significant perturbations at a 1:1 ratio of peptide to hAPE1$^{\Delta N38}$ (not shown).

As shown in Figs. 3 and 4, we mapped the most substantial IDC$_{pep}$-induced chemical shift perturbations on the structure of APE1 [using previously determined crystal structures of free and DNA-bound APE1 [49, 50]]. Intriguingly, many of the residues that physically interact with the IDC are at the DNA-binding site of hAPE1 (Fig. 3). Moreover, many of the residues that physically interact with the IDC surround His309, which is essential for the AP endonuclease activity of hAPE1 [51]. As shown in Fig. 4, binding of the IDC peptide also causes significant chemical perturbations for four residues that are well removed from the DNA-binding site of hAPE1, including H116, Q117, Q137, and C138.

3.2. N212 and Q137 are key mediators of the MYH/APE1 interaction

Based on these NMR data, we sought to verify that both APE1 binding sites are required to facilitate its interaction with MYH. Thus, we constructed two APE1 mutants (APE1-N212A and APE1-Q137A). N212 was chosen for mutagenesis because this residue exhibits the largest chemical shift perturbation at a low IDC:APE1 ratio. Q137 has been shown to exhibit a significant chemical shift perturbation in the presence of the APE1 redox inhibitor RN7–60 [52]. Q137 thus appears to be a part of a potential binding pocket that is located on the opposite side of APE1 relative to its DNA-binding site, and we refer to this site as the “back pocket”. We performed GST-pulldown assays to assess the ability of hMYH(1–350) to interact with purified recombinant wild-type APE1, APE1-N212A, and APE1-Q137A. As shown in Fig. 5A, the N212A and the Q137A APE1 mutants have significantly weaker binding to hMYH(1–350), and the effect is greater for the N212A mutation. The results of triplicate experiments are quantified in Fig. 5B, demonstrating that these differences are statistically significant. In addition, these interactions do not appear to be mediated or influenced by DNA that might have remained during our pulldown procedure. The addition of ethidium bromide (EtBr) is an established technique to distinguish DNA-dependent from DNA-independent interactions [53]. For DNA-dependent interactions, the inclusion of EtBr inhibits the interaction. In a control experiment in the presence of 50 mg/ml EtBr, the amount of APE1 precipitated by GST-hMYH(1–350) was not reduced (Fig. S1), indicating that the MYH/APE1 interaction is DNA-independent. Moreover, the observed decrease in pulldown efficiency was not due to reduced protein stability resulting from the mutations (Fig. 6 and Table 2). Neither the ΔG_{uw} nor the m_{eq} values derived from the chemical denaturation data exhibit statistically-significant differences when comparing wild-type APE1 to the N212A and Q137A mutants. These findings indicate that both the DNA-binding interface and the “back pocket” of APE1 are required for MYH binding.

3.3. The MYH IDC enhances the catalytic activity of APE1

As an additional means to determine the effects of MYH binding to APE1, we measured the steady-state rate of APE1 endonuclease activity (F/G substrate) in the presence and absence

of either the IDC_{pep} or hMYH(65–350). APE1 activity was modestly stimulated by both the IDC_{pep} and hMYH(65–350). Compared to APE1 alone, inclusion of IDC_{pep} increased k_{obs} by 1.7-fold and inclusion of hMYH(65–350) increased k_{obs} by 2.7-fold (Table 3). As a control, we repeated this experiment using BSA at concentrations of 1, 10, and 100 μM in place of hMYH(65–350). BSA had no effect on APE1 activity (Fig. S2A), indicating that the observed stimulation is not likely an artifact resulting from the stabilizing effects of excess protein. The difference in observed catalytic rate for the IDC_{pep} versus hMYH(65–350) reactions is statistically significant, (*p-value* < 0.0001) suggesting that the IDC_{pep} does not fully recapitulate the effect of MYH on the APE1 reaction. However, because the F/G substrate is also a potential MYH reaction product, we felt that the potential interactions between hMYH(65–350) and both intact and cleaved F/G DNA might have impacted the results in some way. Unlike hMYH(65–350), we have no evidence that the IDC_{pep} interacts with DNA, but rather only evidence to the contrary. In particular, creation of a chimeric version of the *Schizosaccharomyces pombe* MYH homologue, SpMyh1, in which the IDC was replaced by the bacterial MutY linker did not alter the binding affinity of SpMyh1 to its abasic product [32]. Moreover, the crystal structure shows that bacterial MutY linker does not contact DNA [54], indicating that it does not contribute to DNA-binding. To address the issue of potential interactions between hMYH(65–350) and the F/G substrate, we repeated the AP-endonuclease experiments using a DNA substrate containing an abasic site opposite thymine (F/T). This substrate does not resemble the MYH reaction product, and thus interactions between hMYH(65–350) and F/T DNA should not contribute to any observed effects. With this substrate, hMYH(65–350) stimulated APE1 endonuclease activity to an extent that was intermediate between that observed for IDC_{pep} and hMYH(65–350) on F/G DNA. In particular, k_{obs} was similar to that observed when using hMYH(65–350) and the F/G DNA (yet the difference in k_{obs} is statistically significant; *p-value* = 0.008), whereas the fold stimulation was lower (2.1- versus 2.7-fold). However, these data do show that hMYH(65–350) can stimulate the AP-endonuclease activity of APE1 without a functional interaction between MYH and the DNA substrate. To ensure that stimulation requires a functional interaction between MYH and APE1, we performed the experiment with APE1-Q137A (see above), hMYH(65–350) and the F/T substrate (Fig. S2B). The impaired interaction between hMYH(65–350) and APE1-Q137A resulted in an attenuated stimulatory effect. hMYH(65–350) was able to stimulate APE1-Q137A activity by 1.4-fold, markedly less than the 2.1-fold stimulation observed for wild-type APE1. APE1-N212A is inactive [55] and therefore was not tested in these experiments. We interpret these findings as corroboration that the MYH IDC binds the DNA-binding site of APE1 as observed by NMR. Intriguingly, this effect is not dependent upon MYH binding to DNA as both the IDC peptide alone and hMYH(65–350) in the presence of F/T DNA show stimulation of APE1 activity. However, the stimulatory effect of MYH on APE1 requires a functional MYH/APE1 interaction and, based on our data using the Q137A mutant, both MYH binding sites on APE1.

3.4. The presence of hHus1 of the 9-1-1 complex enhances the hMYH/hAPE1 interaction

Because APE1 and the Hus1 subunit of 9-1-1 both interact with the IDC, we examined whether APE1 and Hus1 compete for binding to MYH. We performed GST-pulldown assays of hAPE1 with immobilized hMYH(1–350) in the presence of increasing amounts of hHus1. Control pulldown reactions were performed with the hMYH beads and APE1 in the absence of hHus1. Given that hHus1 and hAPE1 have overlapping interaction domains on hMYH, we hypothesized that hHus1 would compete with hAPE for binding to the WT-hMYH(1–350) beads. We predicted that increasing amounts of hHus1 would decrease the amount of hAPE1 precipitated by WT-hMYH(1–350). Surprisingly, the data were inconsistent with our prediction. Our results suggest that hHus1 actually enhances and stabilizes the hMYH/hAPE1 interaction (Figure 7A, top). The overall trend shows that the

presence of hHus1 increases the amount of co-precipitated hAPE1 and quantification of the amount of APE1 recovered in triplicate experiments indicates that these trends are statistically significant (Figure 7B, left). Moreover, the observed stabilization of the MYH/APE1 complex requires a stable interaction between Hus1 and MYH. The hMYH V315A mutant appears to be a selective mediator of protein-protein interactions, as mutation of V315 to alanine impairs the Hus1 interaction [22] but not the APE1 interaction (Fig. S3). When we performed GST-pulldown assays of hAPE1 with immobilized hMYH(1–350)V315A in the presence of increasing amounts of hHus1, the observed stabilization is lost (Fig. 7A, bottom; Fig. 7B). An additional control utilizing Hus1-N1, a fragment of Hus1 that does not interact with MYH (Lu-Chang, unpublished results), also failed to facilitate an increase in precipitated APE1 (Figure S4). Taken together, these results indicate that a stable interaction between Hus1 and MYH aids in the formation and/or retention of the MYH/APE1 complex. Moreover, our *in vitro* results persist in cells. In *Hus1*$^{-/-}$*p21*$^{-/-}$+GFP MEFs, the amount of MYH precipitated using an anti-APE1 antibody is reduced by about 3-fold relative to the same cells in which Hus1 expression is restored (*Hus1*$^{-/-}$*p21*$^{-/-}$+Hus1, Figure 7C). Thus, our results constitute the first evidence that MYH, APE1 and 9-1-1 can form a ternary DNA repair complex.

4. Discussion

While the key players in the BER pathway are well-studied individually, the mechanisms and consequences of their concerted action remain poorly understood. However, it is clear that disruption of the regulatory protein interaction network that governs BER can have deleterious consequences *in vivo* [32]. The “passing the baton” model of DNA repair [9, 56] holds that the product of each reaction in the BER pathway is transferred to the next enzyme in the pathway in order to mitigate the potential mutagenic and cytotoxic properties of these intermediates. The first of these transfers occurs between MYH and APE1, in which APE1 receives the AP-DNA product from MYH. Prior to our studies reported here, a relatively stable complex between MYH and APE1 was detected via pulldown assays [14], and APE1 in large excess (i.e. 100 to 125-fold) was shown to stimulate the activity of MYH [13, 33]. However, despite its critical role in ensuring that AP-DNA does not escape the BER pathway, little information was known regarding the interaction between MYH and APE1. Our current studies have defined key residues of APE1 that facilitate its interaction with MYH.

We demonstrate that hMYH, via its interdomain connector (IDC), binds to APE1 at its DNA-binding site and an additional site that we call the “back pocket”. Our findings on MYH/APE1 interaction may be applied to the interactions of APE1 with other DNA repair proteins. That is, while MYH appears to be the only glycosylase that physically interacts with APE1, APE1 has a number of functional interactions with other DNA repair proteins that likely utilize the binding interfaces identified by these studies.

The finding that hMYH physically interacts with the DNA-binding site of APE1 is surprising and intriguing. The observation that MYH binding is attenuated when N212 is mutated to alanine indicates that this interaction is specific. Although it makes sense that hMYH binds close to the active site of hAPE1 to enable the smooth transfer and immediate processing of AP-DNA, it is unexpected that hMYH binds in such a manner as to occupy the APE1 active site and interact directly N212, a residue required for APE1 activity [55]. Further investigation is needed to better understand how this interaction might facilitate the transfer of AP-DNA from MYH to APE1. Moreover, as hAPE1 interacts with the interdomain connector of hMYH, it is unknown how the two globular N- and C- terminal domains of hMYH are dislodged from AP-DNA. However, these findings can be interpreted in two ways: (1) it might be just a byproduct of hMYH utilizing the only existing APE1

binding interface, or (2) hMYH might stimulate the enzymatic efficiency of hAPE1 through this interaction as part of a *bona fide* BER regulatory mechanism. While our current data shows stimulation of APE1 activity by both the IDC peptide and hMYH(65–350), it is possible that this effect is primarily a consequence of the IDC interacting with the DNA-binding surface of APE1. However, hMYH(65–350) did stimulate hAPE1 activity to a greater extent than the IDC peptide and this stimulation was not dependent upon the opposing base (i.e. F/G versus F/T, see Table 3). Thus, it is also possible that MYH stimulates APE1 activity in some manner after the AP-DNA is transferred from MYH to APE1. Taken together, these observations open up the possibility that a more dynamic interplay between BER enzymes exists at sites of damage than previously envisioned.

Equally intriguing is the role of the APE1 "back pocket" (residues R136, Q137, C138) in MYH binding. This site also happens to be the region of APE1 bound by the redox inhibitor RN7–60 [52], suggesting that this small cavity on the back surface of APE1 might mediate other important APE1 interactions. As in the case of N212, the attenuation of binding upon mutating Q137 to alanine indicates that this is a specific interaction. However, binding is not completely abolished in either case, which raises the possibility that each binding site is not occupied by the same IDC in the complex. While MYH is not known to oligomerize in solution, it typically binds DNA with some positive cooperativity (32, 46–48), indicating that at least two MYH monomers reside on a small (~20 bp) DNA. The functional consequences of cooperative binding behavior are unknown, and the available structural information for bacterial MutY bound to DNA indicates that a monomeric MutY makes all of the required contacts to recognize an A/G° mispair and excise the mispaired adenine. However, the observation of cooperative binding by definition indicates that the multiple binding events are of indistinguishable affinity. Because these binding events are of approximately the same high affinity, they are likely to be functionally significant. This is in contrast to the case of TDG where the second binding event is from 7- to >1300-fold weaker, depending on the substrate; therefore, binding of a second TDG monomer is viewed as lacking functional significance [57]. It is possible that, as suggested for MutY [58, 59], the dimeric form of MYH is the active form, and that APE1 recognizes the MYH dimer using the two binding sites revealed here. In the case of the pulldowns, which do not contain DNA, GST is dimeric (49) and thus could force hMYH(65–350) into a dimeric form, thereby recapitulating this effect to some extent and explaining why neither single mutant completely abolishes wild-type binding. Moreover, it appears that, while each residue contributes to binding, neither is essential for binding. However, because the MYH IDC is 59 residues long, it is possible that both the DNA-binding site and the "back pocket" are occupied simultaneously by a single IDC molecule (and by extension a single molecule of hMYH). In both the monomeric and dimeric binding scenarios, conformational shifts of both MYH and APE1 could play a significant role.

Recent studies have implicated the unstructured N-terminal region of APE1, which comprises roughly the first 40 residues of APE1, in a newly-discovered role in RNA metabolism [60–63]. The function of APE1 in RNA metabolism is mediated by interactions with nucleophosmin (NPM1) and acetylation of five key lysines (K24, K25, K27, K31, and K32) in the unstructured N-terminus [61, 64]. NPM1 can also stimulate AP-site cleavage by APE1, indicating a possible role for both NPM1 and the N-terminal 40 residues of APE1 in DNA metabolism as well [64], In light of these findings, we examined whether the N-terminal 40 residues might influence the MYH/APE1 interaction. GST-pulldown experiments using hMYH(1–350) and both full-length hAPE1 and hAPE1$^{\Delta N38}$ do not exhibit appreciable differences in the amount of APE1 precipitated by MYH (Figure S5). Thus, the N-terminal 40 residues are not required to facilitate the interaction between MYH and APE1. However, while these residues do not appear to be central to the concerted action

of MYH and APE1, that does not preclude the N-terminal 40 residues from having a role in MYH-directed BER.

A prominent theme in BER has been that multi-protein-DNA complexes exist to maximize the efficiency of BER. In such a scenario one protein or several proteins would serve as a central coordinator to mediate the assembly of such complexes. Because of the large number of proteins that interact with both APE1 and the 9-1-1 complex, both proteins have been implicated to carry out this role. However, APE1 has also been reported to have very transient interactions with AP-DNA and forms an even more unstable enzyme-product complex [65]. This rapid dissociation could enable APE1 to associate with and stimulate other BER enzymes assembled at the site of DNA damage via transient and low-affinity interactions with protein-binding partners. Our inability to saturate $APE1^{\Delta N38}$ with IDC_{pep} in NMR experiments suggests that this is a low affinity interaction. However, the interaction is both specific and reproducible using a number of methods, suggesting it is important for function.

The ability of 9-1-1 to stabilize the MYH/APE1 complex might be part of an essential regulatory mechanism in BER. 9-1-1 presumably forms a more a stable complex with DNA, as its heterotrimeric clamp completely encircles DNA. Due to the dual roles of the 9-1-1 complex in BER and DNA-damage response signaling, it may serve as an ideal coordinator, linking the local repair of DNA by BER to a more global, cellular response. Our general model is that MYH first recognizes an A/Go mispair, and then recruits the 9-1-1 complex. In turn, the 9-1-1 complex serves as a platform to assist in the transfer of each product in the BER pathway to its cognate enzyme, culminating in mutation-free DNA. Facilitating the transfer of AP-DNA from MYH to APE1 might be the first of a number of regulatory actions taken by 9-1-1 to ensure completion of repair. Moreover, the presence of a regulatory scaffold like 9-1-1 could facilitate a dynamic interplay between BER enzymes by sequestering them at sites of damage. Such interplay could help ensure that toxic BER intermediates do not escape the pathway and imperil the integrity of the genome.

In summary, our findings suggest that MYH, APE1, and 9-1-1 form a functional unit for efficient BER. MYH activity can be stimulated by APE1 [13, 33] and 9-1-1 [22, 32] while APE1 can be stimulated by MYH and 9-1-1 (Table 3 and [26]). These results are consistent with the hypothesis that the 9-1-1 complex serves as a platform to coordinate the BER pathway. Further study of this regulatory protein interaction network is required to fully elucidate how these protein interactions mitigate the mutagenic potential of oxidative DNA damage.

Supplementary Material

Refer to Web version on PubMed Central for supplementary material.

Acknowledgments

This work was supported funds from the American Cancer Society Research Scholar Grant RSG-09-058-01-GMC (EAT), the Baltimore Excellence in STEM Teaching (BEST) Project (LJL), the Nathan Schnaper Cancer Research Summer Intern Program (SK), National Institutes of Health grants CA 78391 (ALC) and GM 72711 (ACD). The authors would like to thank Dr. Kristen Varney of the University of Maryland, Baltimore NMR Shared Service for assistance with the collection of NMR spectra. We would also like to thank Dr. Robert Weiss (Cornell University) for providing the *Hus1*$^{-/-}$*p21*$^{-/-}$+GFP, and *Hus1*$^{-/-}$*p21*$^{-/-}$+Hus1 mouse embryonic fibrobast cells.

The abbreviations used are

8-oxoG or G°	7,8-dihydro-8-oxoguanine

9-1-1	Rad9-Rad1-Hus1
AP	apurinic/apyrimidinic
APE1	AP-endonuclease 1
BSA	bovine serum albumin
BER	base excision repair
BstMutY	*Bacillus stearothermophilus* MutY
Ec-cMutY	*Escherichia coli* MutY catalytic domain
EtBr	ethidium bromide
F	tetrahydrofuran abasic site analog
GST	glutathione *S*-transferase
h	human
HSQC	heteronuclear spin quantum coherence
IDC	interdomain connector
LP	long-patch
MAP	MYH-associated polyposis
MEF	mouse embryonic fibroblast
MYH or MUTYH	MutY homologue
ODN	oligodeoxynucleotides
S. cerevisiae	*Saccharomyces cerevisiae*
S. pombe	*Schizosaccharomyces pombe*
SN	singlenucleotide patch

References

1. Lindahl T, Wood RD. Quality control by DNA repair. Science. 1999; 286:1897–1905. [PubMed: 10583946]
2. Fan J, Wilson DM 3rd. Protein-protein interactions and posttranslational modifications in mammalian base excision repair. Free Radic Biol Med. 2005; 38:1121–1138. [PubMed: 15808410]
3. Mol CD, Parikh SS, Putnam CD, Lo TP, Tainer JA. DNA repair mechanisms for the recognition and removal of damaged DNA bases. Annu Rev Biophys Biomol Struct. 1999; 28:101–128. [PubMed: 10410797]
4. Almeida KH, Sobol RW. A unified view of base excision repair: lesion-dependent protein complexes regulated by post-translational modification. DNA Repair (Amst). 2007; 6:695–711. [PubMed: 17337257]
5. Gary R, Kim K, Cornelius HL, Park MS, Matsumoto Y. Proliferating cell nuclear antigen facilitates excision in long-patch base excision repair. J Biol Chem. 1999; 274:4354–4363. [PubMed: 9933638]
6. Collins AR. Oxidative DNA damage, antioxidants, and cancer. Bioessays. 1999; 21:238–246. [PubMed: 10333733]
7. Al-Tassan N, Chmiel NH, Maynard J, Fleming N, Livingston AL, Williams GT, Hodges AK, Davies DR, David SS, Sampson JR, Cheadle JP. Inherited variants of MYH associated with somatic G:C-->T:A mutations in colorectal tumors. Nat Genet. 2002; 30:227–232. [PubMed: 11818965]

8. David SS, O'Shea VL, Kundu S. Base-excision repair of oxidative DNA damage. Nature. 2007; 447:941–950. [PubMed: 17581577]

9. Wilson SH, Kunkel TA. Passing the baton in base excision repair. Nat Struct Biol. 2000; 7:176–178. [PubMed: 10700268]

10. Baldwin MR, O'Brien PJ. Human AP endonuclease 1 stimulates multiple-turnover base excision by alkyladenine DNA glycosylase. Biochemistry. 2009; 48:6022–6033. [PubMed: 19449863]

11. Sidorenko VS, Nevinsky GA, Zharkov DO. Mechanism of interaction between human 8-oxoguanine-DNA glycosylase and AP endonuclease. DNA Repair (Amst). 2007; 6:317–328. [PubMed: 17126083]

12. Xia L, Zheng L, Lee HW, Bates SE, Federico L, Shen B, O'Connor TR. Human 3-methyladenine-DNA glycosylase: effect of sequence context on excision, association with PCNA, and stimulation by AP endonuclease. J Mol Biol. 2005; 346:1259–1274. [PubMed: 15713479]

13. Yang H, Clendenin WM, Wong D, Demple B, Slupska MM, Chiang JH, Miller JH. Enhanced activity of adenine-DNA glycosylase (Myh) by apurinic/apyrimidinic endonuclease (Ape1) in mammalian base excision repair of an A/GO mismatch. Nucleic Acids Res. 2001; 29:743–752. [PubMed: 11160897]

14. Parker A, Gu Y, Mahoney W, Lee SH, Singh KK, Lu AL. Human homolog of the MutY repair protein (hMYH) physically interacts with proteins involved in long patch DNA base excision repair. J Biol Chem. 2001; 276:5547–5555. [PubMed: 11092888]

15. Dianova II, Bohr VA, Dianov GL. Interaction of human AP endonuclease 1 with flap endonuclease 1 and proliferating cell nuclear antigen involved in long-patch base excision repair. Biochemistry. 2001; 40:12639–12644. [PubMed: 11601988]

16. Kedar PS, Kim SJ, Robertson A, Hou E, Prasad R, Horton JK, Wilson SH. Direct interaction between mammalian DNA polymerase beta and proliferating cell nuclear antigen. J Biol Chem. 2002; 277:31115–31123. [PubMed: 12063248]

17. Warbrick E. PCNA binding through a conserved motif. Bioessays. 1998; 20:195–199. [PubMed: 9631646]

18. Zhang P, Mo JY, Perez A, Leon A, Liu L, Mazloum N, Xu H, Lee MY. Direct interaction of proliferating cell nuclear antigen with the p125 catalytic subunit of mammalian DNA polymerase delta. J Biol Chem. 1999; 274:26647–26653. [PubMed: 10480866]

19. Dore AS, Kilkenny ML, Rzechorzek NJ, Pearl LH. Crystal structure of the rad9-rad1-hus1 DNA damage checkpoint complex--implications for clamp loading and regulation. Mol Cell. 2009; 34:735–745. [PubMed: 19446481]

20. Sohn SY, Cho Y. Crystal structure of the human rad9-hus1-rad1 clamp. J Mol Biol. 2009; 390:490–502. [PubMed: 19464297]

21. Xu M, Bai L, Gong Y, Xie W, Hang H, Jiang T. Structure and functional implications of the human rad9-hus1-rad1 cell cycle checkpoint complex. J Biol Chem. 2009; 284:20457–20461. [PubMed: 19535328]

22. Shi G, Chang DY, Cheng CC, Guan X, Venclovas C, Lu AL. Physical and functional interactions between MutY glycosylase homologue (MYH) and checkpoint proteins Rad9-Rad1-Hus1. Biochem J. 2006; 400:53–62. [PubMed: 16879101]

23. Guan Y, Manuel RC, Arvai AS, Parikh SS, Mol CD, Miller JH, Lloyd S, Tainer JA. MutY catalytic core, mutant and bound adenine structures define specificity for DNA repair enzyme superfamily. Nat Struct Biol. 1998; 5:1058–1064. [PubMed: 9846876]

24. Guan X, Bai H, Shi G, Theriot CA, Hazra TK, Mitra S, Lu AL. The human checkpoint sensor Rad9-Rad1-Hus1 interacts with and stimulates NEIL1 glycosylase. Nucleic Acids Res. 2007; 35:2463–2472. [PubMed: 17395641]

25. Park MJ, Park JH, Hahm SH, Ko SI, Lee YR, Chung JH, Sohn SY, Cho Y, Kang LW, Han YS. Repair activities of human 8-oxoguanine DNA glycosylase are stimulated by the interaction with human checkpoint sensor Rad9-Rad1-Hus1 complex. DNA Repair (Amst). 2009; 8:1190–1200. [PubMed: 19615952]

26. Gembka A, Toueille M, Smirnova E, Poltz R, Ferrari E, Villani G, Hubscher U. The checkpoint clamp, Rad9-Rad1-Hus1 complex, preferentially stimulates the activity of apurinic/apyrimidinic

endonuclease 1 and DNA polymerase beta in long patch base excision repair. Nucleic Acids Res. 2007; 35:2596–2608. [PubMed: 17426133]

27. Toueille M, El-Andaloussi N, Frouin I, Freire R, Funk D, Shevelev I, Friedrich-Heineken E, Villani G, Hottiger MO, Hubscher U. The human Rad9/Rad1/Hus1 damage sensor clamp interacts with DNA polymerase beta and increases its DNA substrate utilisation efficiency: implications for DNA repair. Nucleic Acids Res. 2004; 32:3316–3324. [PubMed: 15314187]
28. Friedrich-Heineken E, Toueille M, Tannler B, Burki C, Ferrari E, Hottiger MO, Hubscher U. The two DNA clamps Rad9/Rad1/Hus1 complex and proliferating cell nuclear antigen differentially regulate flap endonuclease 1 activity. J Mol Biol. 2005; 353:980–989. [PubMed: 16216273]
29. Wang W, Brandt P, Rossi ML, Lindsey-Boltz L, Podust V, Fanning E, Sancar A, Bambara RA. The human Rad9-Rad1-Hus1 checkpoint complex stimulates flap endonuclease 1. Proc Natl Acad Sci U S A. 2004; 101:16762–16767. [PubMed: 15556996]
30. Smirnova E, Toueille M, Markkanen E, Hubscher U. The human checkpoint sensor and alternative DNA clamp Rad9-Rad1-Hus1 modulates the activity of DNA ligase I, a component of the long-patch base excision repair machinery. Biochem J. 2005; 389:13–17. [PubMed: 15871698]
31. Wang W, Lindsey-Boltz LA, Sancar A, Bambara RA. Mechanism of stimulation of human DNA ligase I by the Rad9-rad1-Hus1 checkpoint complex. J Biol Chem. 2006; 281:20865–20872. [PubMed: 16731526]
32. Luncsford PJ, Chang DY, Shi G, Bernstein J, Madabushi A, Patterson DN, Lu AL, Toth EA. A structural hinge in eukaryotic MutY homologues mediates catalytic activity and Rad9-Rad1-Hus1 checkpoint complex interactions. J Mol Biol. 2010; 403:351–370. [PubMed: 20816984]
33. Pope MA, Chmiel NH, David SS. Insight into the functional consequences of hMYH variants associated with colorectal cancer: distinct differences in the adenine glycosylase activity and the response to AP endonucleases of Y150C and G365D murine MYH. DNA Repair (Amst). 2005; 4:315–325. [PubMed: 15661655]
34. Bennett MT, Rodgers MT, Hebert AS, Ruslander LE, Eisele L, Drohat AC. Specificity of human thymine DNA glycosylase depends on N-glycosidic bond stability. J Am Chem Soc. 2006; 128:12510–12519. [PubMed: 16984202]
35. Manvilla BA, Varney KM, Drohat AC. Chemical shift assignments for human apurinic/apyrimidinic endonuclease 1. Biomol NMR Assign. 2010; 4:5–8. [PubMed: 19888678]
36. Ho SN, Hunt HD, Horton RM, Pullen JK, Pease LR. Site-directed mutagenesis by overlap extension using the polymerase chain reaction. Gene. 1989; 77:51–59. [PubMed: 2744487]
37. Fitzgerald ME, Drohat AC. Coordinating the initial steps of base excision repair. Apurinic/apyrimidinic endonuclease 1 actively stimulates thymine DNA glycosylase by disrupting the product complex. J Biol Chem. 2008; 283:32680–32690. [PubMed: 18805789]
38. Bradford MM. A rapid and sensitive method for the quantitation of microgram quantities of protein utilizing the principle of protein-dye binding. Anal Biochem. 1976; 72:248–254. [PubMed: 942051]
39. Wu Z, Ericksen B, Tucker K, Lubkowski J, Lu W. Synthesis and characterization of human alpha-defensins 4–6. J Pept Res. 2004; 64:118–125. [PubMed: 15317502]
40. Delaglio F, Grzesiek S, Vuister GW, Zhu G, Pfeifer J, Bax A. NMRPipe: a multidimensional spectral processing system based on UNIX pipes. J Biomol NMR. 1995; 6:277–293. [PubMed: 8520220]
41. Goddard, TG.; Kneller, DT. SPARKY. San Francisco: University of California;
42. Cavangh, J.; Fairbrother, WJ.; Palmer, AG., III; Rance, M.; Skelton, NJ. Principles and Practice: Protein NMR Spectroscopy. Elsevier Academic Press; 2007.
43. Manyusa S, Whitford D. Defining folding and unfolding reactions of apocytochrome b5 using equilibrium and kinetic fluorescence measurements. Biochemistry. 1999; 38:9533–9540. [PubMed: 10413531]
44. Santoro MM, Bolen DW. Unfolding free energy changes determined by the linear extrapolation method. 1. Unfolding of phenylmethanesulfonyl alpha-chymotrypsin using different denaturants. Biochemistry. 1988; 27:8063–8068. [PubMed: 3233195]
45. Leatherbarrow, RJ. Grafit 5. Staines, UK: Erithacus Software, Ltd.; 1998.

46. Weiss RS, Matsuoka S, Elledge SJ, Leder P. Hus1 acts upstream of chk1 in a mammalian DNA damage response pathway. Curr Biol. 2002; 12:73–77. [PubMed: 11790307]
47. Parker A, Gu Y, Lu AL. Purification and characterization of a mammalian homolog of Escherichia coli MutY mismatch repair protein from calf liver mitochondria. Nucleic Acids Res. 2000; 28:3206–3215. [PubMed: 10954587]
48. Beernink PT, Segelke BW, Hadi MZ, Erzberger JP, Wilson DM 3rd, Rupp B. Two divalent metal ions in the active site of a new crystal form of human apurinic/apyrimidinic endonuclease, Ape1: implications for the catalytic mechanism. J Mol Biol. 2001; 307:1023–1034. [PubMed: 11286553]
49. Gorman MA, Morera S, Rothwell DG, de La Fortelle E, Mol CD, Tainer JA, Hickson ID, Freemont PS. The crystal structure of the human DNA repair endonuclease HAP1 suggests the recognition of extra-helical deoxyribose at DNA abasic sites. Embo J. 1997; 16:6548–6558. [PubMed: 9351835]
50. Mol CD, Izumi T, Mitra S, Tainer JA. DNA-bound structures and mutants reveal abasic DNA binding by APE1 and DNA repair coordination [corrected]. Nature. 2000; 403:451–456. [PubMed: 10667800]
51. Barzilay G, Mol CD, Robson CN, Walker LJ, Cunningham RP, Tainer JA, Hickson ID. Identification of critical active-site residues in the multifunctional human DNA repair enzyme HAP1. Nat Struct Biol. 1995; 2:561–568. [PubMed: 7664124]
52. Manvilla BA, Wauchope O, Seley-Radtke KL, Drohat AC. NMR studies reveal an unexpected binding site for a redox inhibitor of AP endonuclease 1. Biochemistry. 2011; 50:10540–10549. [PubMed: 22032234]
53. Lai JS, Herr W. Ethidium bromide provides a simple tool for identifying genuine DNA-independent protein associations. Proc Natl Acad Sci U S A. 1992; 89:6958–6962. [PubMed: 1495986]
54. Lee S, Verdine GL. Atomic substitution reveals the structural basis for substrate adenine recognition and removal by adenine DNA glycosylase. Proc Natl Acad Sci U S A. 2009; 106:18497–18502. [PubMed: 19841264]
55. Rothwell DG, Hickson ID. Asparagine 212 is essential for abasic site recognition by the human DNA repair endonuclease HAP1. Nucleic Acids Res. 1996; 24:4217–4221. [PubMed: 8932375]
56. Prasad R, Shock DD, Beard WA, Wilson SH. Substrate channeling in mammalian base excision repair pathways: passing the baton. J Biol Chem. 2010; 285:40479–40488. [PubMed: 20952393]
57. Morgan MT, Maiti A, Fitzgerald ME, Drohat AC. Stoichiometry and affinity for thymine DNA glycosylase binding to specific and nonspecific DNA. Nucleic Acids Res. 2011; 39:2319–2329. [PubMed: 21097883]
58. Lee CY, Bai H, Houle R, Wilson GM, Lu AL. An Escherichia coli MutY mutant without the six-helix barrel domain is a dimer in solution and assembles cooperatively into multisubunit complexes with DNA. J Biol Chem. 2004; 279:52653–52663. [PubMed: 15456766]
59. Wong I, Bernards AS, Miller JK, Wirz JA. A dimeric mechanism for contextual target recognition by MutY glycosylase. J Biol Chem. 2003; 278:2411–2418. [PubMed: 12441341]
60. Barnes T, Kim WC, Mantha AK, Kim SE, Izumi T, Mitra S, Lee CH. Identification of Apurinic/apyrimidinic endonuclease 1 (APE1) as the endoribonuclease that cleaves c-myc mRNA. Nucleic Acids Res. 2009; 37:3946–3958. [PubMed: 19401441]
61. Lirussi L, Antoniali G, Vascotto C, D'Ambrosio C, Poletto M, Romanello M, Marasco D, Leone M, Quadrifoglio F, Bhakat KK, Scaloni A, Tell G. Nucleolar accumulation of APE1 depends on charged lysine residues that undergo acetylation upon genotoxic stress and modulate its BER activity in cells. Mol Biol Cell. 2012; 23:4079–4096. [PubMed: 22918947]
62. Tell G, Wilson DM 3rd, Lee CH. Intrusion of a DNA repair protein in the RNome world: is this the beginning of a new era? Mol Cell Biol. 2010; 30:366–371. [PubMed: 19901076]
63. Vascotto C, Fantini D, Romanello M, Cesaratto L, Deganuto M, Leonardi A, Radicella JP, Kelley MR, D'Ambrosio C, Scaloni A, Quadrifoglio F, Tell G. APE1/Ref-1 interacts with NPM1 within nucleoli and plays a role in the rRNA quality control process. Mol Cell Biol. 2009; 29:1834–1854. [PubMed: 19188445]
64. Fantini D, Vascotto C, Marasco D, D'Ambrosio C, Romanello M, Vitagliano L, Pedone C, Poletto M, Cesaratto L, Quadrifoglio F, Scaloni A, Radicella JP, Tell G. Critical lysine residues within the

overlooked N-terminal domain of human APE1 regulate its biological functions. Nucleic Acids Res. 2010; 38:8239–8256. [PubMed: 20699270]

65. Wilson DM 3rd, Takeshita M, Demple B. Abasic site binding by the human apurinic endonuclease, Ape, and determination of the DNA contact sites. Nucleic Acids Res. 1997; 25:933–939. [PubMed: 9023101]

Highlights

- MYH interacts specifically with APE1 via a region of MYH that we call the interdomain connector (IDC)
- The MYH IDC specifically contacts two distinct regions of APE1
- MYH can stimulate the enzymatic activity of APE1, indicating an unanticipated level of crosstalk between the two enzymes
- Stabilization of the MYH/APE1 complex by Hus1 represents the first evidence that all three proteins exist in a complex.

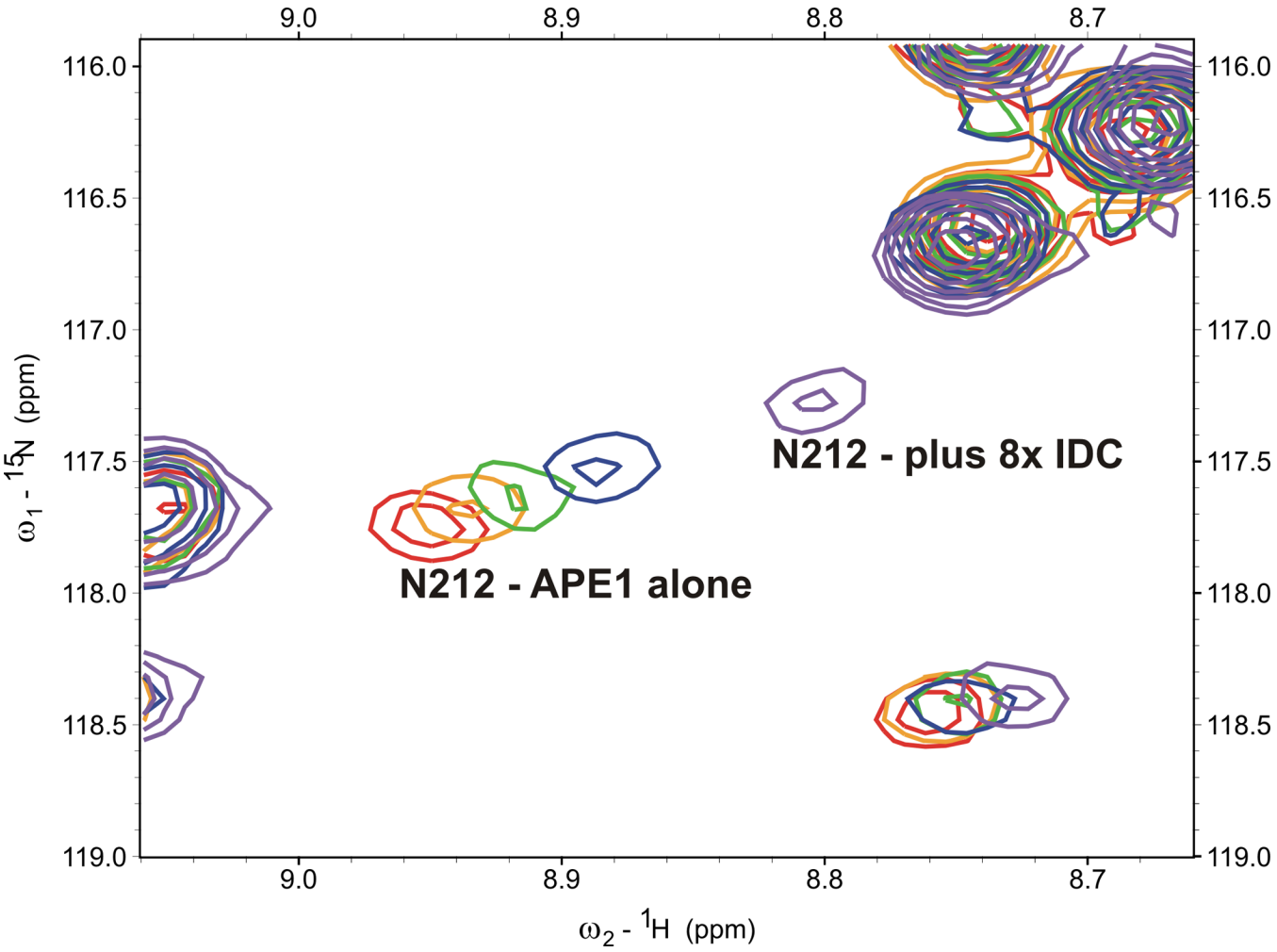

Figure 1. NMR Titration Experiment of $^{15-}$ N-hAPE1$^{\Delta N38}$ with the hMYH IDC peptide shows a significant shift in residue N212

The HSQC of five NMR spectra of hAPE1$^{\Delta N38}$ are overlaid. The control experiment of hAPE1$^{\Delta N38}$ (200 μM) alone is shown in red Additional NMR spectra were collected in the presence of increasing amounts of the hMYH IDC peptide. The spectra for hAPE1$^{\Delta N38}$ and the IDC peptide in molar ratios of 1:1 (orange), 1:2 (green), 1:4 (blue), and 1:8 (purple) are shown. Residue N212 is located at the DNA-binding site of hAPE1$^{\Delta N38}$ and also interacts with the hMYH IDC peptide as shown by the significant chemical shift perturbations.

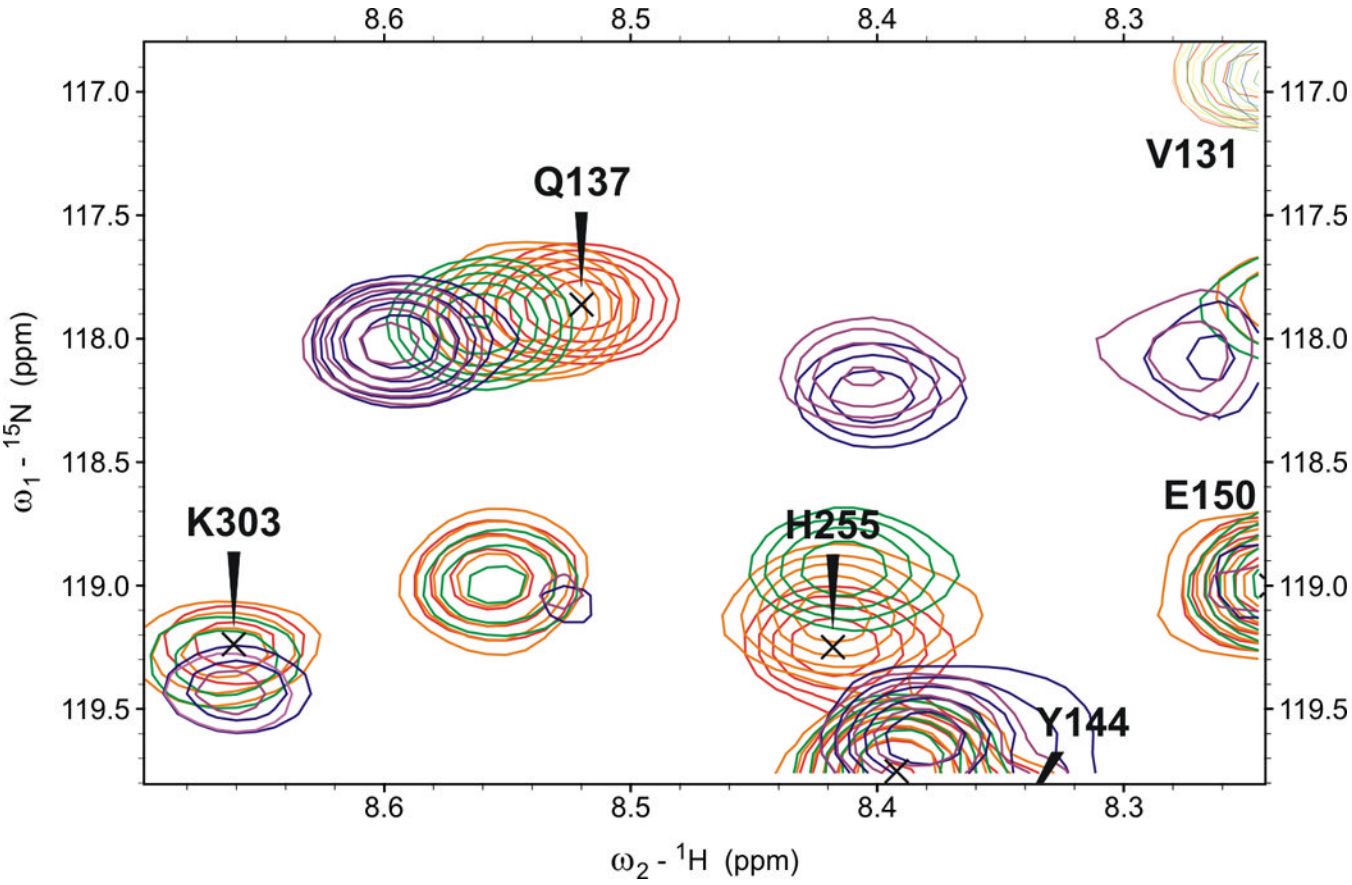

Figure 2. NMR Titration Experiment of $^{15-}$ N-hAPE1$^{\Delta N38}$ with the hMYH IDC peptide shows a significant shift in residue Q137

The control experiment of hAPE1$^{\Delta N38}$ (200 μM) alone is shown in red and the subsequent titrations (APE1:IDC 1:1, 1:2, 1:4, 1:8) are shown in orange, green, blue, and purple. Residues Q137, K303, H255, Y144, E150, and V131 are indicated.

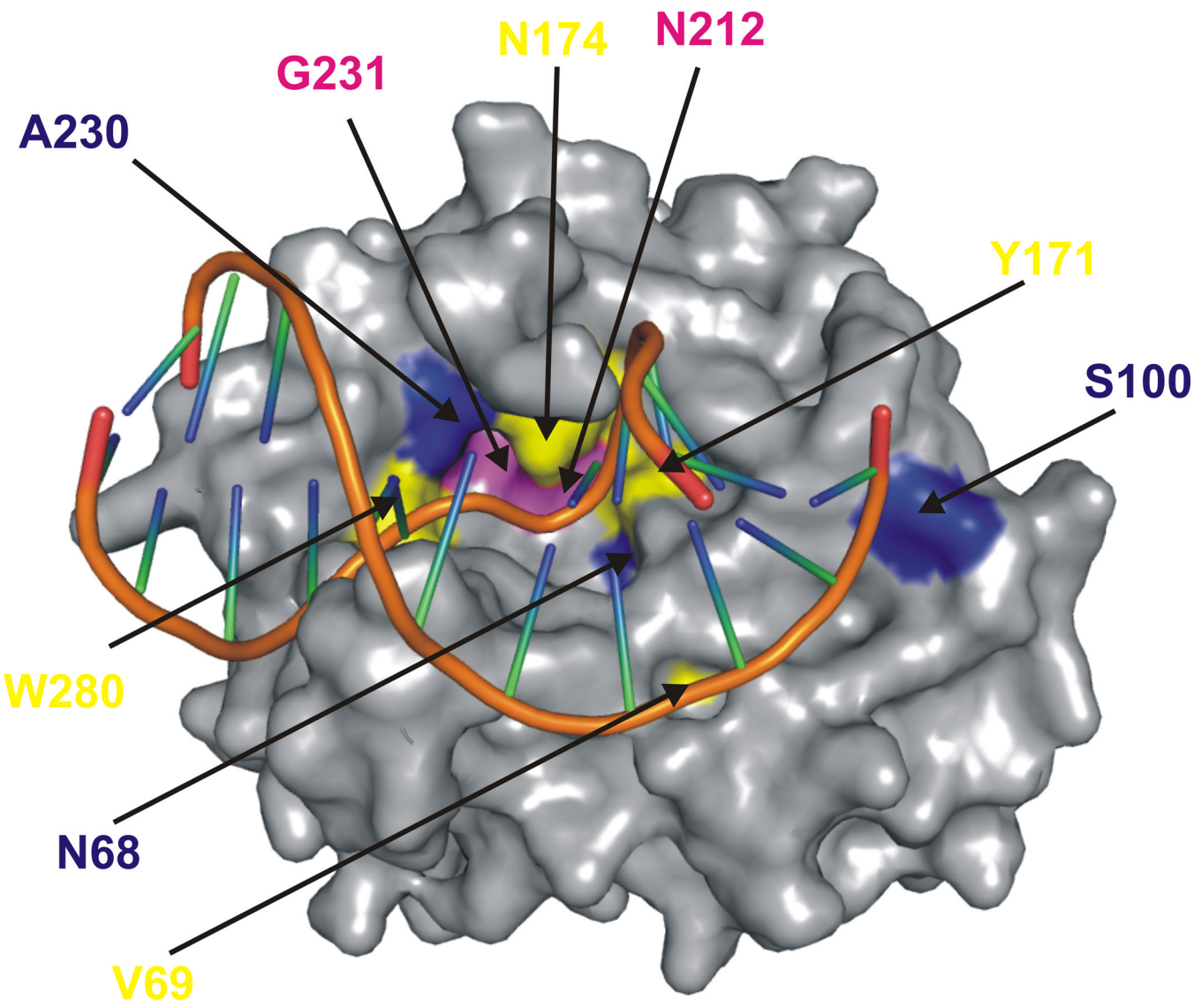

Figure 3. The hMYH interdomain connector physically interacts with the DNA binding site of hAPE1

The apo-hAPE1(36–318) (PDB ID: 1BIX) and the AP-DNA-hAPE1(40–318) (PDB ID: 1DE8) crystal structures by Gorman *et al*.[49] and by Mol *et al*.[50], respectively, were used to map hAPE1 residues that shifted the most in the presence of the IDC peptide during our NMR experiments. Many of the hAPE1 residues that interact with the IDC are at the DNA-binding site. Residues N212 and G231 are shown in magenta and experienced significant chemical shift perturbations at even a 1:1 molar ratio of IDC to hAPE1$^{\Delta N38}$. Residues V69, Y171, N174, W280, and L282 are shown in yellow and showed significant chemical shift perturbations starting at a 2:1 ratio of IDC to hAPE1$^{\Delta N38}$. Residues N68, S100, and A230 also exhibited chemical shift perturbations beginning at a 4:1 ratio of IDC to hAPE1$^{\Delta N38}$ and are colored blue.

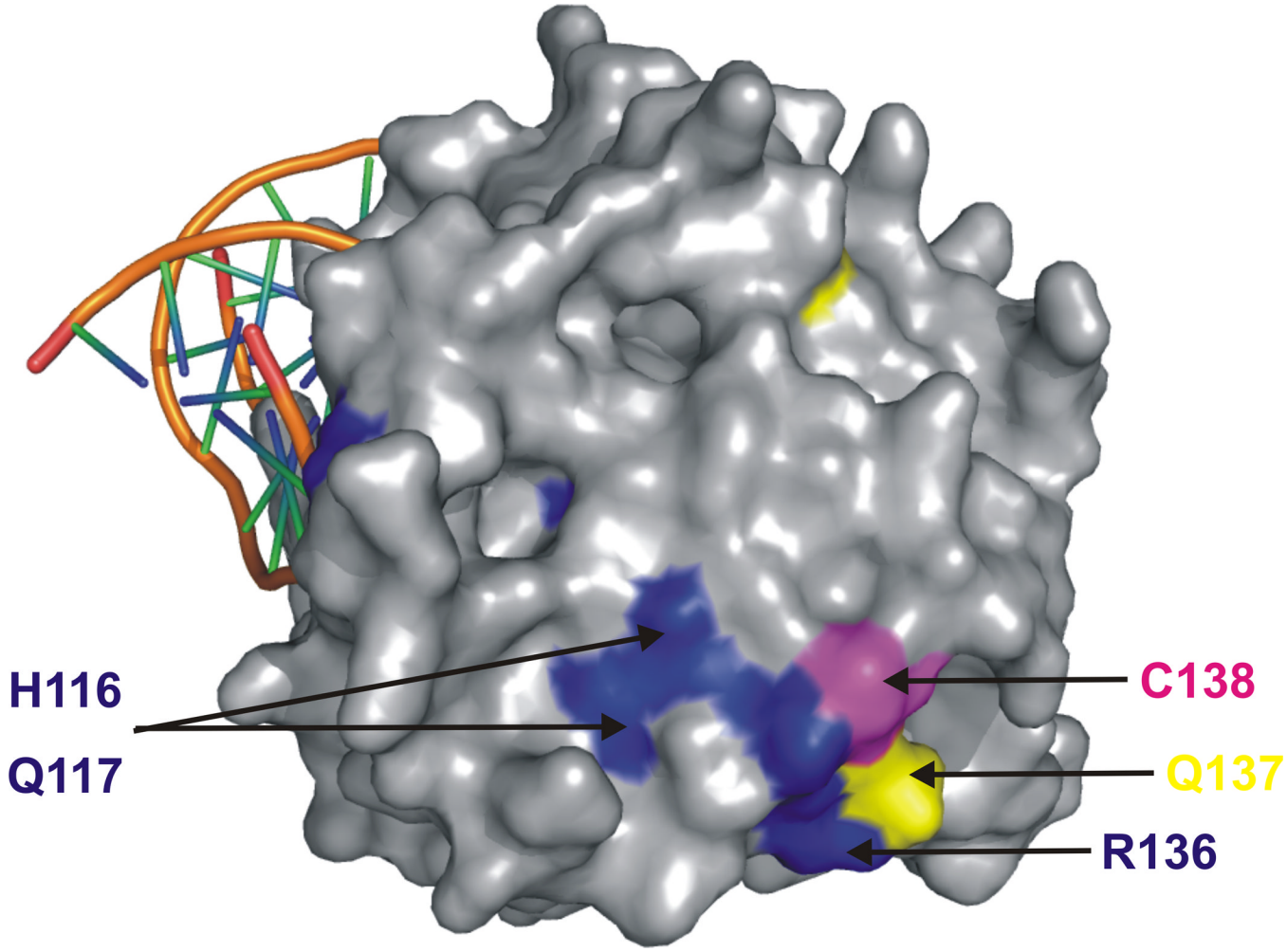

Figure 4. The hMYH interdomain connector also physically interacts with the "back pocket" of hAPE1

Residues Q137 (yellow) and C138 (magenta) exhibited the largest chemical shift perturbations and are shown on the opposite face of hAPE1 from its DNA-binding site. Residues H116, Q117, and R136 exhibit smaller chemical shift perturbations and are shown in blue. Although different in magnitude, each of these residues had significant chemical shift perturbations in the 2 IDC: 1 hAPE1$^{\Delta N38}$ spectra compared with the control spectra.

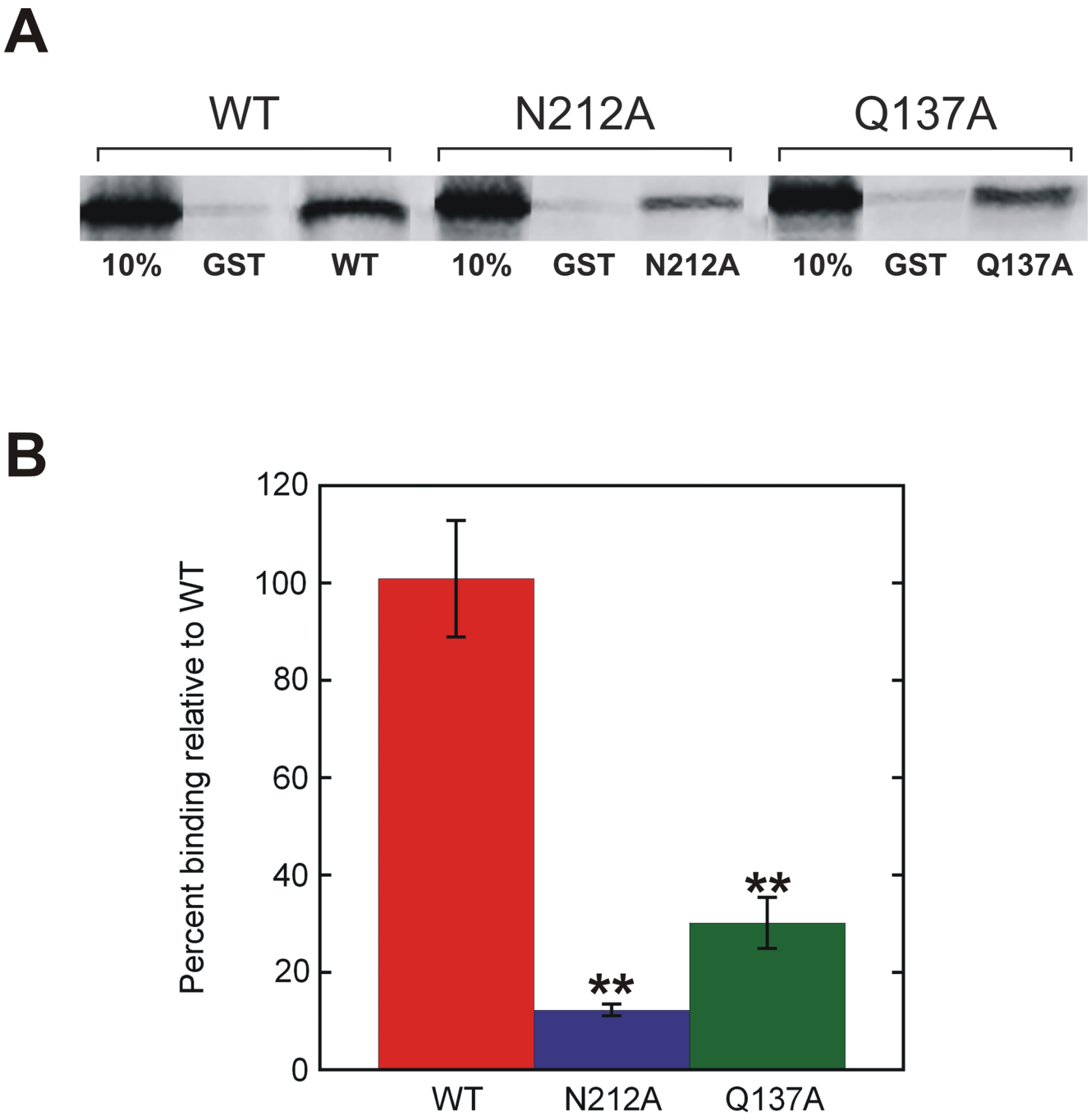

Figure 5. The N212A and Q137A mutations of hAPE1 attenuate the hMYH/hAPE1 interaction

(A) GST-pull down assays were performed with GST-tagged- WT-hMYH(1–350) immobilized to glutathione-sepharose beads. 200 ng of APE1 (WT, N212A, or Q137A as indicated) were incubated with the beads for 2 hours before thoroughly washing with buffer containing 0.2% NP-40 and 0.3M NaCl. Both the supernatant (not shown) and the pellets were fractionated by SDS-PAGE and Western blot analysis was performed with Anti-hAPE1 antibody (Abcam). 10% input of APE1 is shown as a reference.

(B) Quantitation of triplicate pulldown experiments. Statistical significance was assessed with an unpaired t-test. ** indicates a *p-value* of less than 0.001.

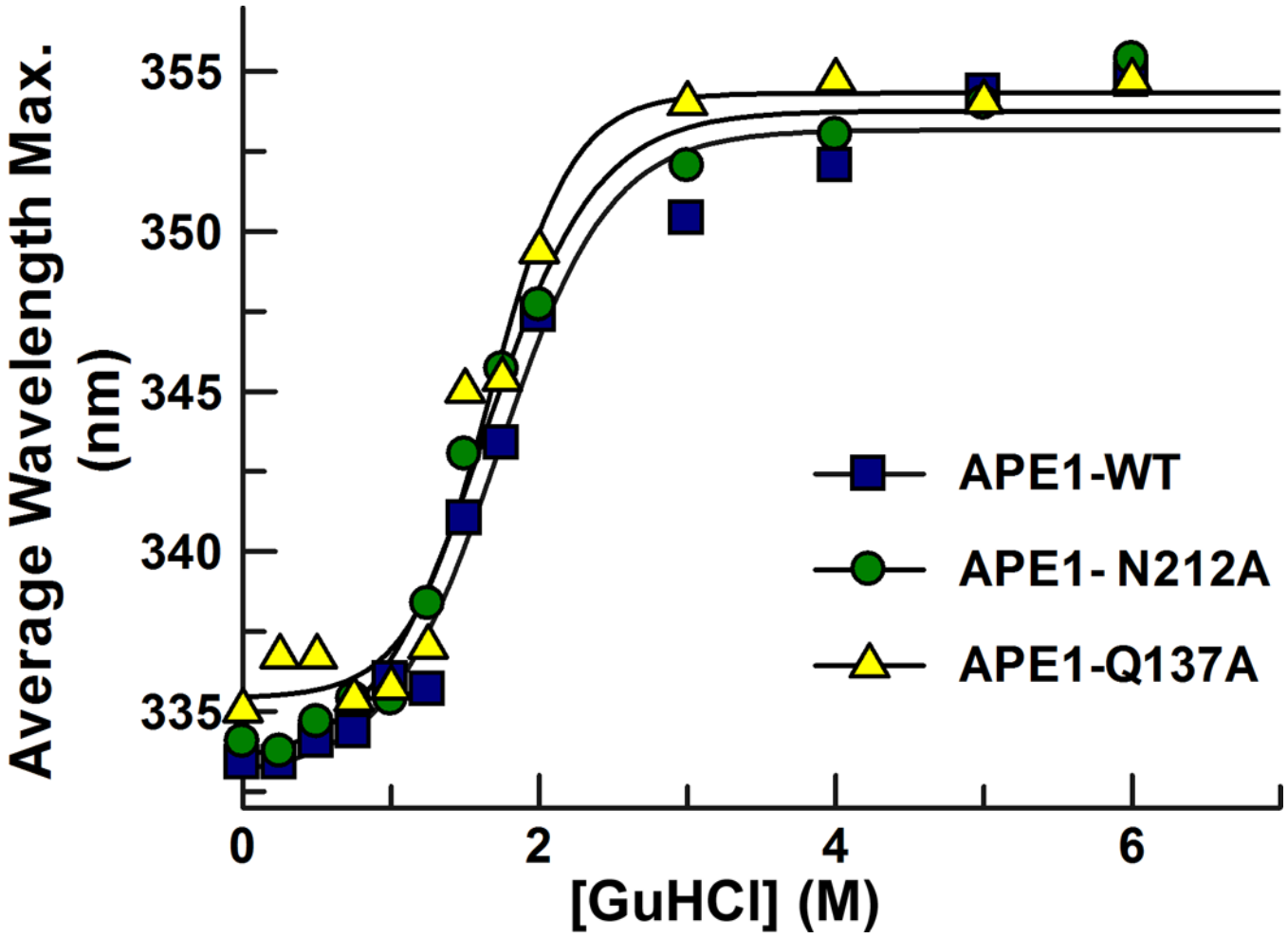

Figure 6. APE1-WT, APE1-N212A, and APE1-Q137A do not differ in stability

Representative profiles of the wavelength at which maximal fluorescence emission from excited tryptophan residues is observed as a function of GuHCl concentration. Solid lines indicate the best fit of each profile to Equation 2.

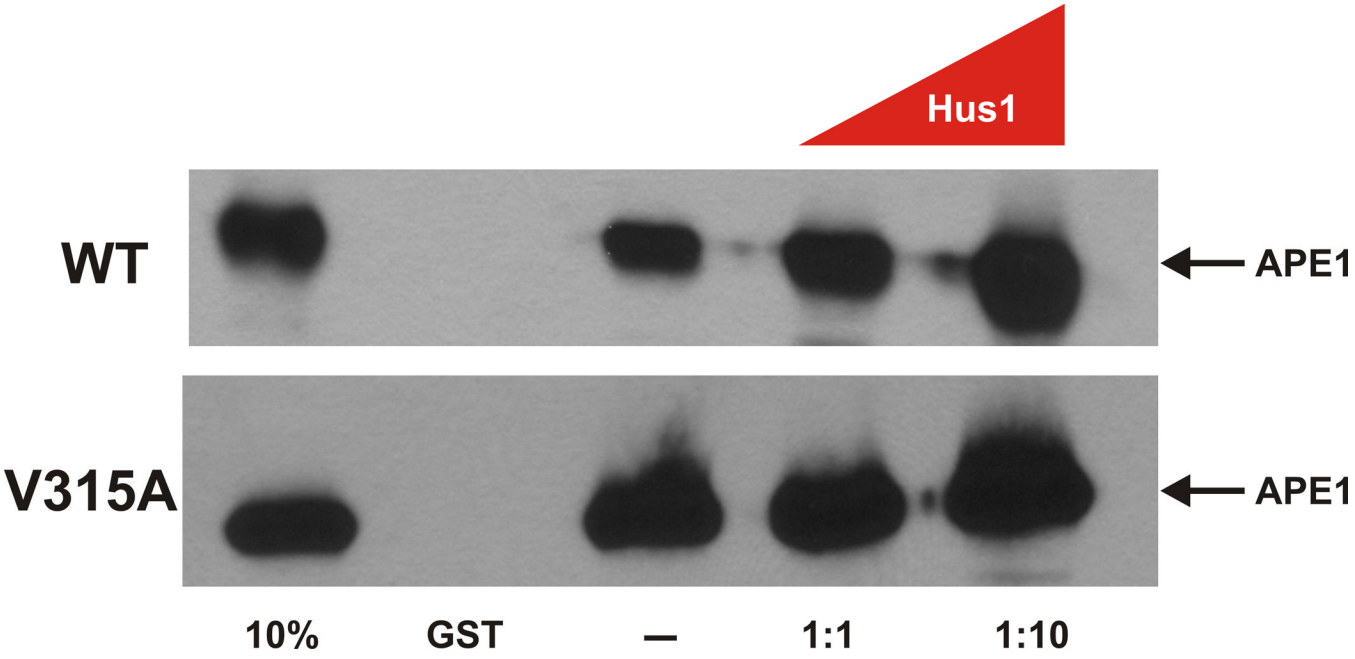

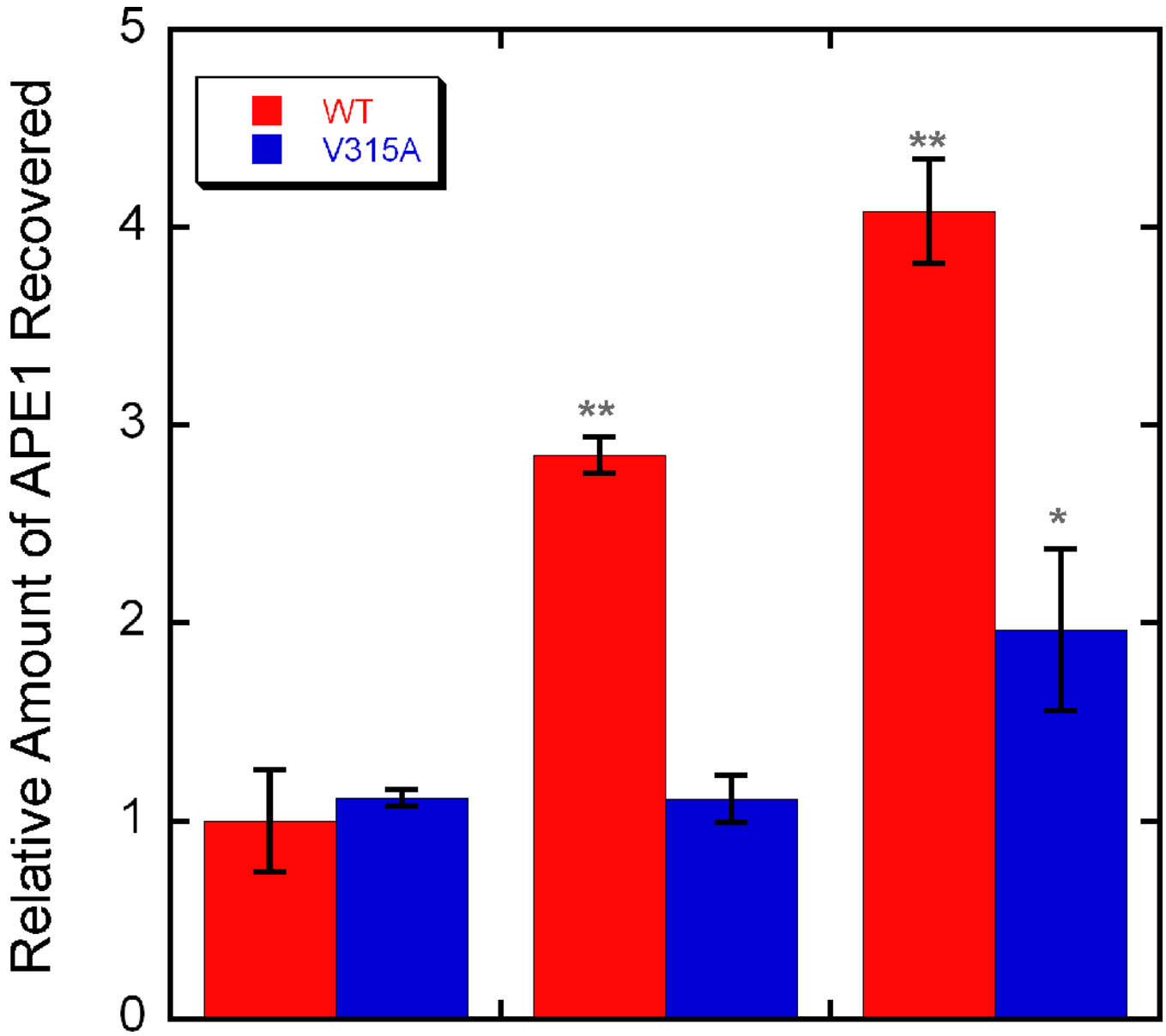

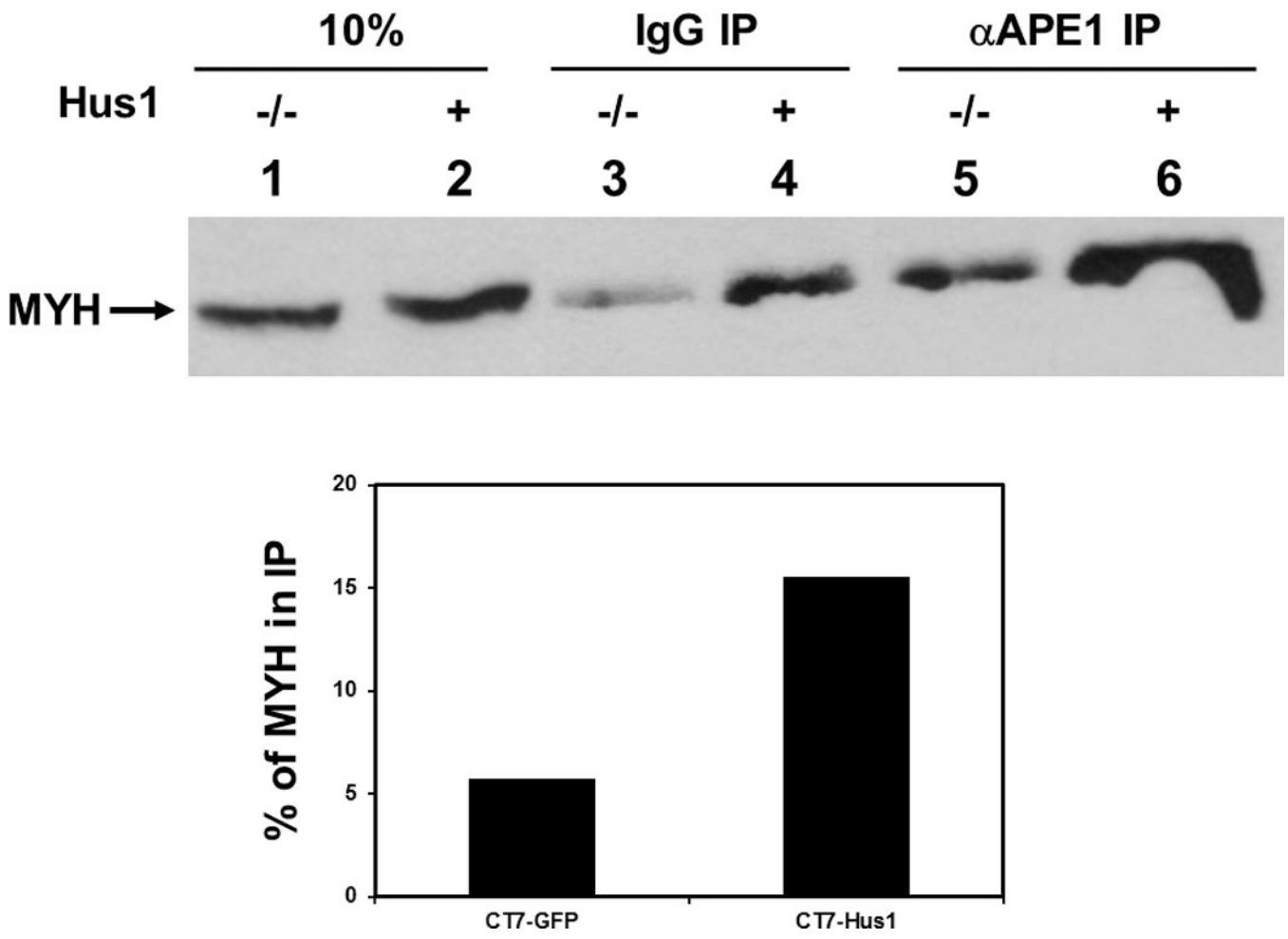

Figure 7. hHus1 stabilizes the hMYH/hAPE1 interaction

(A) GST-pull down assays were performed with GST-tagged wild type hMYH(1–350) (lanes 3 −5, top) or hMYH(1–350)-V315A (lanes 3 –5, bottom) protein immobilized to glutathione-sepharose beads. 200 ng of APE1 (~ 5 pmol) were incubated in each of the reactions in the presence of increasing amounts of hHus1. The reaction shown in lane 3 was incubated with a 1:1 hHus1 to APE1 molar ratio, corresponding to 5 pmol of hHus1. Lane 5 shows the reaction incubated with 10:1 hHus1 to APE1, corresponding to 50 pmol of hHus1. A control pulldown reaction was perfomed in the absence of hHus1 (lane 3). The reactions were incubated with rocking overnight at 4°C and then washed thoroughly with buffer containing 0.1% NP-40 before completing Western blot analysis with Anti-hAPE1 antibody (Abcam). Lane 1 shows 10% input of APE1.

(B) Quantitation of triplicate pulldown experiments. Statistical significance was assessed with an unpaired t-test. ** indicates a *p-value* of less than 0.001. * indicates a *p-value* of less than 0.05.

(C) Co-immunoprecipitation of MYH from *Hus1*$^{-/-}$*p21*$^{-/-}$ (or CT7) MEFs using an anti-APE1 antibody. Lanes 1 and 2 represent 10% input of MYH in the *Hus1*$^{-/-}$*p21*$^{-/-}$+GFP (CT7-GFP) and *Hus1*$^{-/-}$*p21*$^{-/-}$+Hus1 (CT7-Hus1) cells, respectively. Similarly, lanes 3 and 4 show the amount of MYH precipitated using the control IgG antibody in both cell lines. Finally, lanes 5 and 6 show the amount of MYH precipitated using the anti-APE1 antibody using both cell lines. Below is shown the quantification of lanes 5 and 6. When

Hus1 expression is restored, approximately three times as much MYH precipitates with APE1 relative to the knockout.

Table 1

Chemical shifts for hAPE1 $^{\Delta N38}$-free and with a 2-fold molar equivalent of IDC_{pep}.

Residue	δ $^{15-}$N (ppm), no IDC	δ $^{15-}$ N (ppm), 2x IDC	δ^{1-} H (ppm), no IDC	δ^{1-} H (ppm), 2x IDC	Δδ (ppm)
N212	117.75	117.68	8.95	8.94	0.016
C138	127.54	127.46	8.81	8.82	0.015
G231	117.90	117.86	6.07	6.08	0.014
H116	123.65	123.54	7.78	7.78	0.013
Q137	117.86	117.88	8.51	8.52	0.012
Q117	123.29	123.33	7.82	7.83	0.011
W280SC	131.44	131.49	9.91	9.91	0.009
E216	117.65	117.60	9.67	9.66	0.006
V172	130.40	130.38	7.83	7.82	0.004

Table 2

Stability of APE1 WT, N212A, and Q137A

Protein	ΔG_{uw}	m_{eq}
APE1 WT	2.7 ± 0.6	1.6 ± 0.3
APE1 N212A	2.5 ± 0.4	1.6 ± 0.2
APE1 Q137A	3.5 ± 0.8	2.2 ± 0.4

The results shown are the mean ± standard deviation for three independent experiments.

Table 3

Stimulation of hAPE1 $^{\Delta N38}$ AP-endonuclease activity by the hMYH IDC and hMYH(65–350).

Sample	DNA	k_{obs} (s^{-1})	Standard Deviation
APE1 alone-1	F/G	0.298	0.007
APE1 + IDC_{pep}	F/G	0.503	0.007
APE1 alone-2	F/G	0.210	0.010
APE1 + MYH(65–350)	F/G	0.576	0.001
APE1 alone-3	F/T	0.301	0.006
APE1 + MYH(65–350)	F/T	0.624	0.017

The results shown are the mean and standard deviation for three independent experiments. In each experiment, a duplex DNA of 17 base pairs with the indicated centrally-located abasic site analog was used at a concentration of 1 μM.